IEEE Access
Multidisciplinary | Rapid Review | Open Access Journal

Received August 29, 2019, accepted September 14, 2019, date of publication September 24, 2019, date of current version October 8, 2019.

Digital Object Identifier 10.1109/ACCESS.2019.2943422

Development of Nonlinear Electromechanical Coupled Macro Model for Electrostatic MEMS Cantilever Beam

AKANKSHA D. SINGH, (Student Member, IEEE), AND RAJENDRA M. PATRIKAR, (Senior Member, IEEE)
Centre for VLSI and Nanotechnology, Visvesvaraya National Institute of Technology, Nagpur 440010, India
Corresponding author: Akanksha D. Singh (akankshasingh222@gmail.com)

This work was supported by the Indian Nanoelectronics User Program (INUP), IIT Bombay, through the DIT, MCIT, and Government of India.

ABSTRACT The deployment of MicroElectroMechanical System (MEMS) cantilever in the electronic systems is continuously increasing. These devices are usually interfaced with electronic circuits. It is important to build its macro model for rapid system design and simulation. This paper proposes development of an electromechanical coupling macro model of electrostatically actuated MEMS cantilever for straight and curled beam configurations. It consists of linear electrical components and nonlinear dependent sources, which represent mechanical parameters and electromechanical coupling in the system. In order to model device mechanics, analytical formulations are done and calculations are adapted to macro model. A methodology to derive electromechanical coupling as a function of bias voltage is developed. This electrical model is capable of predicting the device characteristic behaviour before the onset of pull-in instability region and estimates pull-in voltage. Such macro model can be easily implemented in any circuit simulation platform and be used to demonstrate the possible advantage of using this scheme for device and system dynamics optimization. To arrive at equivalence, an analytical formulation for spring constant and pull-in voltage of cantilever based on the partial load distribution and curling is derived. It utilizes the methodology based on nonlinear electrostatic pressure approximated by its linearized uniform counterpart and mechanical force-deflection model. An electrical characterization of fabricated MEMS cantilever is done to obtain the experimental value of pull-in voltage. Simulation Program with Integrated Circuit Emphasis (SPICE) simulations results for the developed model is obtained for actual device dimensions and is in good agreement with analytical and experimental results.

INDEX TERMS Electrostatic devices, macro model, microelectromechanical systems.

I. INTRODUCTION

Microelectromechanical systems (MEMS) has revolutionized the sensor industry by combining silicon-based microelectronics with micromachining technology. Microcantilevers form a major device clan for its use as sensors and also as actuators. The application field of electrostatic MEMS cantilevers has widened covering multidisciplinary areas like Pixelled antenna [1], MEMS tunable filter [2], aerospace microsystems [3], biomedical systems like automatic DNA samplers [4], video display projectors like Digital Light Processor (DLP), etc. Its increasing deployment in such sophisticated systems has led to immediate need for consideration of entire MEMS at higher abstraction levels such as schematic and system ones. At these levels, a low-order behavioural representation of the MEMS devices known as macro models can be utilized. For many applications, it is convenient to build macro models by equivalent circuit representation approach [5], [6]. We will utilise the same in our analysis.

The equivalent circuit representation approach benefits from lower computation time and explicit physical realization and analyses of systems consisting of complex structural components and coupled subsystems. It also provides an approach to gain the acumen of the dynamic behaviour of the system [7]. When we establish the

The associate editor coordinating the review of this manuscript and approving it for publication was Hassen Ouakad.

equivalent circuit representation, we can utilize the circuit simulators, like SPICE for simulation of circuits based on the micro-cantilevers.

The currently available techniques include the multi-physics computer-aided design (CAD) tools [8], experimental observations and analytical calculations. The CAD tools are largely based on the finite element method to simulate the mechanical behaviour and function at device or component level as a function of electrical stimuli. An electrical circuit simulator acts as multi-physics platform to simulate behavior of MEMS actuator or sensor by utilizing lumped/ distributed element modelling in single electrical domain [9].

In the lumped element model, the mass, compliance, capacitance, etc. can be easily recognized at individual points and have finite degree of freedom whereas, in distributed element model, it is continuously distributed throughout the system and has infinite degree of freedom. The distributed parameter system is a lumped parameter system with an infinite number of mechanical ports, one for each mode of vibration [10]. In the resonance mode, the equivalent circuit of the distributed parameter system can be approximated by a circuit representing a single-degree-of-freedom lumped parameter system. Thus, we conclude that the distributed element model is a complex version of the lumped element model with a refinement of results obtained with it. In this work, we focus on the static mode of operation of the device, hence the lumped parameter modelling is utilized to simulate the behavior of MEMS actuator/sensor.

The developed electrical model should capture the characteristic phenomenon inherited by the devices. In this paper, we deal with electrostatically actuated MEMS cantilevers, which offers quick response, lower power consumption, simplicity of design, fabrication and integration with the integrated circuit process. However, the major setback affecting the system performance is Pull-in instability [11], which is an inherent characteristic of MEMS electrostatically actuated devices. This is because of the rapid increase in the nonlinear electrostatic force than linear restoring force resulting in collapse of the cantilever beam on the fixed bottom electrode. This causes saddle-node bifurcation called Pull-in, which limits beam travel range to one-third of the total range. The actuation voltage at which the beam loses its stability and enters the unstable region is Pull-in voltage. The pull-in voltage acts similar to the threshold voltage and is thus required to be modelled in the circuit design.

The surface micromachining process for fabrication of MEMS cantilever introduces imperfections in the structure. Due to stress gradients, initial curling is observed in beam, which causes the change of equilibrium configuration and variation of system parameters such as pull-in voltage and resonant frequencies [12]. For reliable system operation, calibration of beam curling is required. Thus, electrical modelling of curling is required.

In this work, we have developed an accurate macro model using electrical equivalent circuit approach for electrostatically actuated MEMS cantilever for utilization in straight and curled beam configurations. To establish electromechanical coupling in the macro model, it is important to model the transduction factor. We present a method for the accurate determination of the transduction factor including the spring softening effect modelled using a spring softening capacitor. It can be used to simulate the mechanical behaviour of the MEMS cantilever beam under any electrical excitation in a circuit simulator. Equivalent circuit models for transducers [5]–[7], [9], [10], [13], [14], Capacitive Micromachined Ultrasonic Transducers [15] have been developed, however efforts to electrically model MEMS cantilever are not reported much. The electrical model is able to uniquely evaluate the performance of the MEMS cantilever beam through its pull-in induced behaviour by predicting Pull-in voltage without the need for fitting.

The analytical derivation of Pull-in voltage for MEMS cantilever is done based on uniform pressure approximation of nonlinear electrostatic pressure and the mechanical force-deflection model for curled and straight beams. The analytical, experimental and circuit simulation results are in good agreement with each other. The macro model has also been verified for its operation with experimental and analytical values available in the literature and are found to be in agreement with its results.

The measurement of the total gap due to initial gap and offset deflection (due to curling) of the fabricated devices is done by Scanning Electron Microscope (SEM), which is then fed as input to equivalent circuit. The circuit simulation output well matches with the curled device characterization results. However, no fitting was used either in the model or in experiments for the purpose of comparison.

The rest of the paper is organized as follows. Section 2 deals with modelling aspects for partial distribution based electrostatically actuated MEMS cantilever namely beam stiffness, its macro model is developed in section 3. Section 4 deals with model parameter evaluation. This is followed by fabrication and electrical characterization of MEMS cantilever in section 5. Circuit simulation results are discussed in section 6 followed by model validation and discussion in section 7. Finally, we conclude in section 8.

II. CONVENTIONAL MECHANICAL MODELLING

The MEMS cantilever structure consists of two electrodes as depicted in Fig. 1(a), where upper deformable plate of length L, width b and thickness t forms top electrode and fixed bottom plate of length L_e and width b forms the bottom electrode. L_a is the distance between anchor and bottom electrode. These two plates are electrically biased to develop an attractive electrostatic force. This force displaces the top electrode from its original position, thus causing a change in capacitance. Therefore, it is possible to change the displacement of the deformable plate through voltage control of the gap between two plates.

Fig. 1(b) shows the mechanical model for electrostatic MEMS cantilever represented as spring-mass-dashpot assembly, for which m, c, k are mass of deformable electrode,

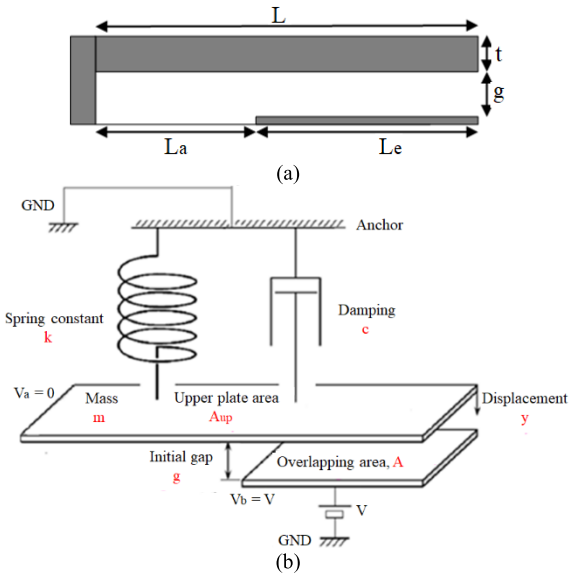

FIGURE 1. Electrostatically actuated MEMS cantilever (a) Structure (b) Mechanical model.

damping co-efficient and spring constant respectively. It is driven by voltage source V developing electrostatic force F_e. Let A be overlapping plate area, g the initial air gap, y is the tip deflection due to applied voltage and ϵ is permittivity in the gap.

The governing equation of motion (EOM) of lumped parameter model of MEMS cantilever beam subjected to electrostatic loading [9] is given as

$$m\ddot{y} + c\dot{y} + ky = F_e \tag{1}$$

where overdot represents derivative with respect to time.

The electrostatic force developed is given [16] by

$$F_e = \frac{1}{2}\frac{\varepsilon A}{(g-y)^2}V^2 \tag{2}$$

It is nonlinear and inversely proportional to the distance between the electrodes. When the deformable electrode deflects under the electrostatic force, the distance between them further reduces. F_e becomes discontinuous at the point, where beam touches bottom electrode, as there is abrupt variation in derivative of capacitance. Thus, nonlinear behaviour extends from electrostatic forces to the electromechanical response of MEMS cantilever beam causing loss of stability and limitation in range of stable states.

So (1) becomes

$$m\ddot{y} + c\dot{y} + ky = \frac{1}{2}\frac{\varepsilon A}{(g-y)^2}V^2 \tag{3}$$

Although closed-form of expression for the applied voltage and the resulting displacement cannot be obtained, a solution is possible by determining the intersection of nonlinear electrostatic force and mechanical restoring force.

It must be taken into consideration that electrostatic force is partially distributed over the free end of cantilever. Therefore, the beam spring constant i.e. stiffness needs to be derived. The stiffness expression is derived at the position of the maximum deflection y_L of cantilever i.e. at its tip [18]. The stiffness $k(\mathrm{Nm}^{-1})$ is defined as fL_e/y_L, where f is distributed transverse load per unit length over partial length L_e originating from the tip of the cantilever beam as shown in Fig. 2.

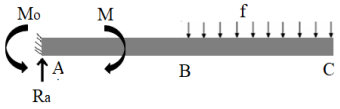

FIGURE 2. Free body diagram of partially actuated beam.

The moment of inertia, I ($I = \frac{bt^3}{12}$) and Young's modulus, E is constant over the whole length of beam. For wide beams (b > 5t), $\tilde{E}$ is equal to the plate modulus $\tilde{E} = E/(1-\vartheta^2)$ where ϑ is Poisson's ratio of beam material.

In order to develop the model, we construct a free body diagram with applied force, moment and reaction force acting on the beam.

Since there is partial load distribution, apart from the moment about anchor position, moment has to be determined separately in region with and without load. We determine the deflection y(x) and hence the stiffness by using linear Euler-Bernoulli differential equation and direct integration.

According to the Euler Bernoulli law [9], bending moment along the length is proportional to change in curvature produced by applied load.

For small deflections [3],

$$\frac{\partial^2 y}{\partial x^2} = y'' = -\frac{M}{\tilde{E}I} \tag{4}$$

The bending moment expression for two different regions and displacement of the beam along its entire length is derived as given below:

For Region $(0 < x < L_a)$*:*

$$M = f\,(L-L_a)\left((x-L_a) - \frac{L-L_a}{2}\right) \tag{5}$$

$$y'' = \frac{f\,(L-L_a)}{\tilde{E}I}\left(x - \frac{L+L_a}{2}\right) \tag{6}$$

We integrate (6) twice by considering appropriate boundary conditions, which yields

$$y = \frac{f\,(L-L_a)\,x^2}{12\tilde{E}I}\,[2x - 3(L-L_a)] \tag{7}$$

For Region $(L_a < x < L)$*:*

$$M = f\,(L-L_a)\left[(x-L_a) - \frac{L-L_a}{2}\right] - \frac{f\,(x-L_a)^2}{2} \tag{8}$$

$$y'' = \frac{f}{\tilde{E}I}\left[Lx - \frac{L^2}{2} - \frac{x^2}{2}\right] \tag{9}$$

We integrate (9) twice and solve for appropriate boundary conditions, which yields

$$y = \frac{f}{2\tilde{E}I}\left[\frac{Lx^3}{3} - \frac{L^2x^2}{2} - \frac{x^4}{12} + \frac{L_a^3 x}{3}\right] + c_4 \tag{10}$$

At x = L_a, deflection y for portion AB and BC must be identical in order to secure continuous deflection curve at point B. Therefore, using x = L_a and equating (7) and (10), we get,

$$y = \frac{f}{24\tilde{E}I}\left[4Lx^3 - 6L^2x^2 - x^4 + 4L_a^3x - L_a^4\right] \quad (11)$$

The beam stiffness is expressed as

$$k = \frac{fL_e}{y_L} = \frac{2\,(L - L_a)\,\tilde{E}bt^3}{3L^4 - 4L_a^3L + L_a^4} \quad (12)$$

The static calculations of cantilever bending are used to define elements in the model.

III. MACRO MODEL

We utilise the equivalent circuit representation approach to build a macro model of the MEMS cantilever beam. The mechanical and electrical circuit equivalents [8] of cantilever are depicted in Fig. 3. Mathematically, forced motion of cantilever can be expressed as

$$\text{Mechanical model}: \quad m\ddot{y} + c\dot{y} + ky = F \quad (13)$$

$$\text{Electrical model}: \quad L\ddot{q} + R\dot{q} + \frac{1}{C}q = V \quad (14)$$

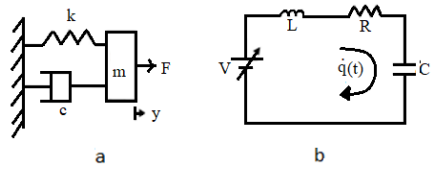

FIGURE 3. Equivalent model of Cantilever (a) Mechanical, (b) Electrical.

The above two models are analogous since both are second-order differential equations with constant coefficients. This is force-voltage analogy.

It allows efficient modelling of the interaction between the electrical and non-electrical components of the system and provides access to the prevailing set of tools for electrical circuits for advanced analyses.

The dynamical behaviour of these elements can be fully described in a single energy domain (e.g. mechanical). Other devices, such as electrostatic actuators, piezoelectric actuators, etc. are best characterized by models that span two or more energy domains. In such cases, multi-domain coupling (such as electromechanical, piezoelectric, etc.) needs to be considered [5], [8], which can be introduced in electrical circuit via controlled sources or transformer.

The electrical model for electrostatically actuated MEMS cantilever using through and across variables is given in Fig.4. The mechanical part is represented on the right side with C_m as beam compliance, L_m as mass of beam and R_m as damping [13]. The velocity is 'through' variable, whereas force is 'across' variable. The electrical part is on the left side where MEMS cantilever behaves like non-linear capacitor,

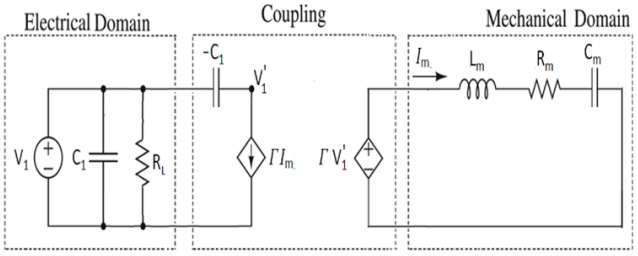

FIGURE 4. Nonlinear Electromechanical coupled Macro model of electrostatically actuated MEMS cantilever using equivalent circuit approach.

C_1 in shunt with voltage source. The total instantaneous capacitance C_1 is voltage-dependent and comprises of static capacitance, C_o and voltage-dependent terms. This capacitor's value depends on instantaneous beam displacement. Both parts are coupled by nonlinear dependent current source (G_2) on left and dependent voltage source (E_2) on right. E_2 represents electrostatic force F_e developed with the application of bias voltage. A leakage resistor, R_L models surface current effect and is placed on the electrical side. The surface leakage current flows due to the generation of electric field between the contact pads of cantilever and bottom electrode and increases with voltage. The spring softening of beam is a coupled field effect and is modelled mathematically as if it was a negative capacitance [18] by series capacitance, $-C_1$ referred to electrical side.

The spring softening effect can be understood from EOM by expanding (3) using Taylor series approximation about a nominal distance y_0 following method outlined in [19]. Simplifying and rearranging, we obtain

$$m\ddot{y} + c\dot{y} + \left(k - \frac{\varepsilon AV^2}{(g - y_0)^3}\right)y = \frac{1}{2}\frac{\varepsilon A}{(g - y_0)^2}V^2 \quad (15)$$

It is observed that electrostatic force modifies stiffness by acting against mechanical spring thus lowering the effective stiffness, k^* leading to spring softening effect.

The transduction factor (Γ) is expressed [7] as

$$\Gamma = \frac{\varepsilon AV}{(g - y_0)^2} \quad (16)$$

From (15) and (16), effective stiffness in terms of transduction factor becomes

$$k^* = k - k_s = k - \frac{(g - y_0)\,\Gamma^2}{\varepsilon A} \quad (17)$$

k^* can then be modelled electrically as

$$k^* = \frac{1}{C_m} - \frac{\Gamma^2}{C_1} = \frac{1}{C_{eff}} \quad (18)$$

The beam remains mechanically stable till $k > k_s$, after which beam instability occurs causing pull-in. Implementing k^* i.e. C_{eff} in the circuit requires two capacitors in series on the mechanical side. On the mechanical side, $-C_1/\Gamma^2$ is a complex function of voltage but when referred to electrical

side becomes $-C_1$. Hence, k* i.e. C_{eff} is implemented by keeping C_m on mechanical and $-C_1$ on the electrical side.

The circuit operates as follows. With the application of voltage, capacitance increases. Meanwhile, dependent voltage source couples voltage from the electrical side with beam mechanics via its transduction factor developing electromechanical force. This initiates the current flow in the mechanical side. This current is coupled back to the electrical side via dependent current source. This brings the series negative capacitance, $-C_1$ into effect, which along with C_m forms effective capacitance, C_{eff}. C_{eff} determines the mechanical stability of beam and nature of current flow. This makes the total circuit interdependent. At pull-in voltage, mechanical instability occurs indicated by high abrupt current flow.

In this section, we derive the expressions for lumped circuit components and transduction factor.

A. LUMPED PARAMETER ESTIMATION

The cantilever exerts a linear restoring force determined by its compliance modelled using capacitance, C_m given as

$$C_m = \frac{1}{k} = \frac{3L^4 - 4L_a^3 L + L_a^4}{2\,(L - L_a)\,\tilde{E} b t^3} \tag{19}$$

Since 'through' variable is selected as velocity, the model inductance L_m that conserves energy is mass of beam [7] given as

$$L_m = m = \rho L b t \tag{20}$$

where ρ is density of beam material.

As can be seen from the electrical side, the MEMS cantilever behaves like a capacitor, which is a dynamic element whose value depends on instantaneous beam displacement and hence applied voltage [20]. Also, it depends on the initial curvature of beam induced due to residual stress from the fabrication process.

Let σ be initial offset deformation due to beam curvature. The total instantaneous capacitance consists of static component, voltage-dependent terms and curvature dependent terms and is of form

$$C_1(V, \sigma) = \frac{\in A}{(g + \sigma)} \sum_{n=0}^{6} a_n e^{b_n (g+\sigma)} V_1^n \tag{21}$$

A sixth-order polynomial with coefficients $a_0, a_1, a_2, \ldots, a_6$ and $b_0, b_1, b_2, \ldots, b_6$ is considered for better prediction of nonlinear behaviour. These coefficients are determined by performing coupled field analysis on finite element software COMSOL Multiphysics followed by polynomial fitting. The stationary analysis is performed and capacitance is extracted at each applied voltage and initial curvature through parametric sweep. The Capacitance-Voltage (C-V) curve is plotted as in fig. 5.

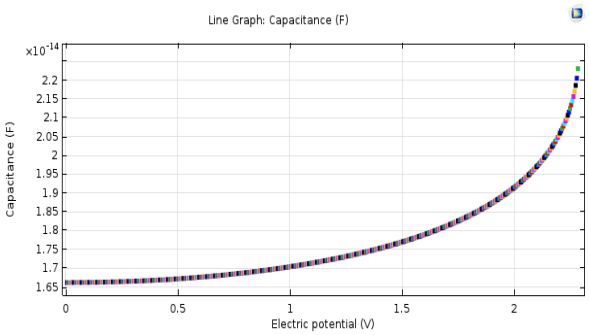

FIGURE 5. Point graph of capacitance vs. voltage in COMSOL for $\sigma = 0$.

B. TRANSDUCTION FACTOR

The electromechanical coupling is modelled by dependent sources with Γ as transduction factor. It is the ratio of electromechanical force generated in response to the voltage applied. The applied voltage, in this case, is not bias voltage since there is spring softening capacitance in series with it. The spring softening is coupled field effect, which cannot be ignored. Thus, the transduction factor with applied voltage, V_1' can be given as

$$\Gamma = \frac{F_e}{V_1'} \tag{22}$$

The operation of electrostatically actuated MEMS cantilever is majorly capacitive. So, we simplify Fig. 4 in terms of purely capacitive elements and calculate the applied voltage V_1' from voltage division network formed because of spring softening capacitance $-C_1$ as

$$V_1' = \frac{\frac{1}{j\omega\Gamma^2 C_m}}{\frac{1}{j\omega\Gamma^2 C_m} - \frac{1}{j\omega C_1}} V_1 = \frac{1}{1 - \Gamma^2 \frac{C_m}{C_1}} V_1 \tag{23}$$

From (22) & (23),

$$\Gamma = \frac{F_e}{V_1}\left(1 - \Gamma^2 \frac{C_m}{C_1}\right) \tag{24}$$

The factor F_e/V_1 is the ratio of electromechanical force generated to bias voltage, denoted as Γ'. This can be extracted from FEM simulator, COMSOL as it takes into consideration the coupled field effect of spring softening. We performed coupled field parametric analysis to get F_e corresponding to each value of bias voltage. The voltage is swept in small step size to get a better accuracy. Γ' can be calculated by taking the ratio of force difference between two successive analyses to voltage step size.

Substituting Γ' and rearranging (24) we get

$$\Gamma'^2 \frac{C_m}{C_1}\left(\frac{\Gamma}{\Gamma'}\right)^2 + \left(\frac{\Gamma}{\Gamma'}\right) - 1 = 0 \tag{25}$$

The above quadratic equation is solved for positive roots to obtain Γ.

It is noted that Γ is dependent on cantilever material, physical dimensions and applied voltage.

We compute Γ' and Γ for fixed dimensions and compare them for each bias voltage. It is observed that Γ' rises rapidly and tends to become infinite as pull-in voltage is reached. However, from (25), it is clear that at the pull-in voltage, Γ has a finite maximum value given by

$$\Gamma_{(pi)} = \sqrt{\frac{C_{1(pi)}}{C_m}} \tag{26}$$

The final circuit is simulated in circuit simulation software SPICE.

IV. MODEL PARAMETER EVALUATION

This section deals with the derivation of closed-form model of pull-in voltage taking into consideration partial electrode effect, fringing field capacitance and curling phenomenon of beam. An approach based on nonlinear electrostatic pressure approximated by its linearized uniform counterpart and mechanical force-deflection model [19] is used for derivation.

As beam deflects, charge redistributes, which causes electrostatic force to increase non-uniformly. Also, for partial electrode configuration, only the free end of cantilever experiences electrostatic force. Remaining portion experiences force due to fringing capacitance effect, which is also small and non-uniform. As a result, the free end of the cantilever experiences more attractive force and electrostatic pressure compared to region near the fixed end as shown in Fig. 6.

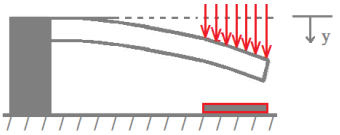

FIGURE 6. Non-uniform electrostatic pressure for cantilever.

The non-uniformity of electrostatic forces causes stiffness of cantilever to change introducing spring softening term, k_s as given in (17) to form effective stiffness, k^*. k_s is expressed by taking into consideration the fringing field effect following the Meijs and Fokkemma model [21] and curling effect [22] as

$$k_s = \frac{\epsilon_o V^2 L_e}{L(g+\sigma\left(\frac{x}{L}\right)^2)}\left[\frac{1}{2(g+\sigma\left(\frac{x}{L}\right)^2)^2} + \frac{0.17}{(g+\sigma\left(\frac{x}{L}\right)^2)^{1.25} b^{0.75}} + \frac{0.4t^{0.5}}{(g+\sigma\left(\frac{x}{L}\right)^2)^{1.5} b} + \frac{0.17}{(g+\sigma\left(\frac{x}{L}\right)^2)^{1.25} L_e^{0.75}}\right] \tag{27}$$

The last three terms takes into consideration the fringing field capacitance developed due to beam width, thickness and free end of beam.

The non-uniform electrostatic pressure, $P_{electrostatic}$ takes into account k_s and is represented by its linearized uniform approximate model about zero deflection point [20] as

$$P_{electrostatic} = \frac{\epsilon_o V^2 L_e}{L}\left[\frac{1}{2(g+\sigma\left(\frac{x}{L}\right)^2)^2} + \frac{0.1325}{(g+\sigma\left(\frac{x}{L}\right)^2)^{1.25} b^{0.75}} + \frac{0.265t^{0.5}}{(g+\sigma\left(\frac{x}{L}\right)^2)^{1.5} b} + \frac{0.1325}{(g+\sigma\left(\frac{x}{L}\right)^2)^{1.25} L^{0.75}}\right] + \frac{k_s y}{A} \tag{28}$$

The geometric nonlinearity effect due to beam curvature has a substantial effect on actuation response of system only if the ratio of initial air-gap to beam length, g/L > 0.09 [11]. In the present analysis, we consider MEMS cantilever having g/L < 0.09.

So, neglecting nonlinear curvature effect, electrostatic pressure is given as

$$P_{electrostatic} = \frac{\epsilon_o V^2 L_e}{L}\left[\frac{1}{2(g+\sigma)^2} + \frac{0.1325}{(g+\sigma)^{1.25} b^{0.75}} + \frac{0.265t^{0.5}}{(g+\sigma)^{1.5} b} + \frac{0.1325}{(g+\sigma)^{1.25} L^{0.75}}\right] + \frac{k_s y}{A} \tag{29}$$

The expression for uniform pressure resulting in cantilever tip deflection is derived using load-deflection model as

$$P_{elastic} = \frac{ky}{bL} \tag{30}$$

At pull-in, pull-in displacement, $y_{pi} = \frac{1}{3}y$.

So, from (28), electrostatic pressure at pull-in, $P_{ele-stat-PI}$ is expressed as

$$P_{ele-stat-PI} = \frac{\epsilon_o L_e V_{pi}^2}{L}\left[\frac{5}{6(g+\sigma)^2} + \frac{0.19}{(g+\sigma)^{1.25} b^{0.75}} + \frac{0.19}{(g+\sigma)^{1.25} L^{0.75}} + \frac{0.4t^{0.5}}{(g+\sigma)^{1.5} b}\right] \tag{31}$$

The pull-in elastic pressure can be evaluated from (30) as

$$P_{PI-elastic} = \frac{k(g+\sigma)}{3bL} \tag{32}$$

Equating (31) and (32),

$$V_{PI} = \sqrt{\frac{2\breve{E}t^3(g+\sigma)}{3\epsilon_o\left(3L^4 - 4L_a^3 L + L_a^4\right)\left(\frac{5}{6(g+\sigma)^2} + \frac{0.19}{(g+\sigma)^{1.25} b^{0.75}} + \frac{0.19}{(g+\sigma)^{1.25} L^{0.75}} + \frac{0.4t^{0.5}}{(g+\sigma)^{1.5} b}\right)}} \tag{33}$$

Equation (33) gives the expression of the pull-in voltage.

The MEMS cantilever is fabricated and details of the fabrication process are described in the next section. The theoretical calculations for the fabricated beam properties given in Table 1 and Table 2 yield the values of mechanical spring constant as 0.625. The pull-in voltage of the straight and curled MEMS cantilever beam is calculated as 2.29V and 6.12V.

TABLE 1. Fabricated device properties.

Structural Elements	Dimensions(in μm)	Material
Cantilever beam	100 x 45 x 0.75	Aluminium
Bottom electrode	40 x 45 x 0.1	Aluminium
Initial gap (straight beam)	0.8	Air
Initial Gap (curled beam)	1.55	Air

TABLE 2. Aluminium properties used.

Young's Modulus, E	70 GPa
Poisson's Ratio, ϑ	0.33
Density, ρ	2700 kg/m^3

V. FABRICATION AND CHARACTERIZATION

MEMS fabrication process involves three steps i.e. film deposition, lithography and etching. Employing surface micromachining technique, five-level lithography process flow is developed as shown in Fig. 7 to fabricate the MEMS cantilever [23]. The top view of fabricated MEMS cantilever after each processing level is shown in Fig. 8. The process begins with deposition of SiO_2 as isolation layer on top of p-type <100> silicon wafer of high resistivity using thermal oxidation. The structural layers of cantilever and bottom electrode are deposited with Aluminium using thermal evaporation. The first level lithography and etching forms bottom electrode. Next, photoresist, which acts as a sacrificial layer is deposited by spin coater and patterned to form cavity for anchor pad. This is followed by Aluminium deposition and third-level patterning to fill the anchor cavity. Fourth level lithography is required to remove remnant photoresist from anchor. Aluminium deposition and 5th level patterning is done for cantilever formation. Finally, cantilevers are released by stripping off sacrificial layer by dipping it in acetone and then desiccating it. The dimension of the fabricated device is given in Table 1. Fig. 9 gives the SEM image of a top view of the fabricated cantilever device. Fig. 10 gives a side view of two set of cantilever devices. In fig. 10 (a), straight cantilever beam can be observed with an initial gap of 0.8μm, whereas in fig. 10 (b), MEMS cantilever is curled due to stress gradients developed during fabrication giving a total gap of 1.55μm.

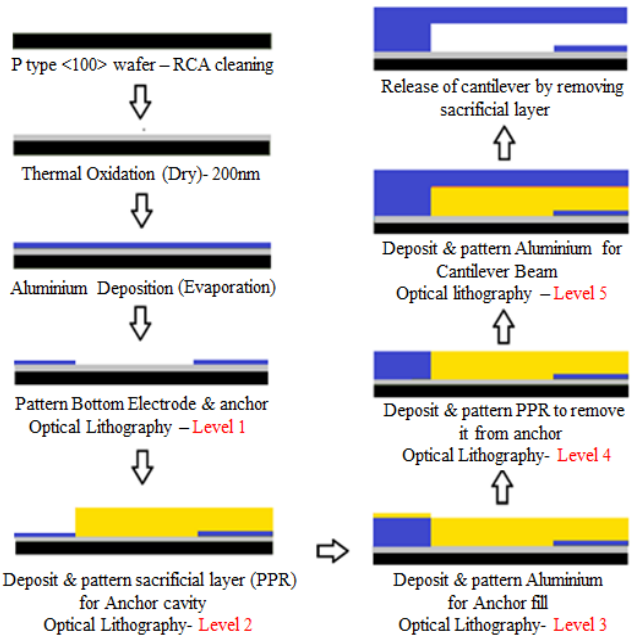

FIGURE 7. Fabrication flow of MEMS cantilever.

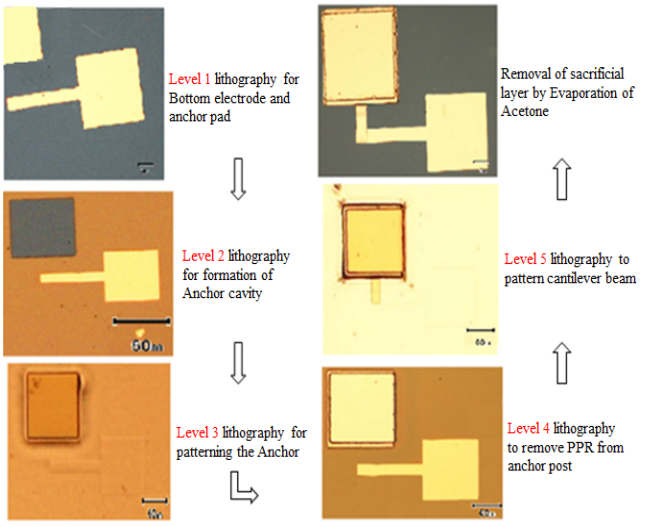

FIGURE 8. Top view of the fabricated structure after each lithographic level and final release of beam.

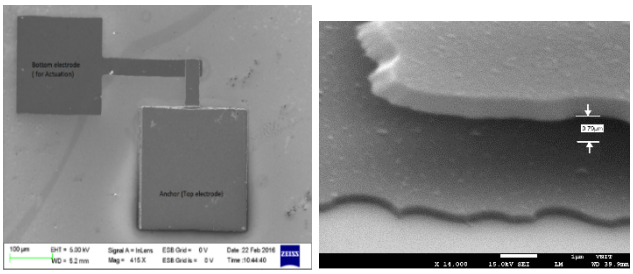

FIGURE 9. SEM image of (a) top view of fabricated device (b) gap between two electrodes (free end).

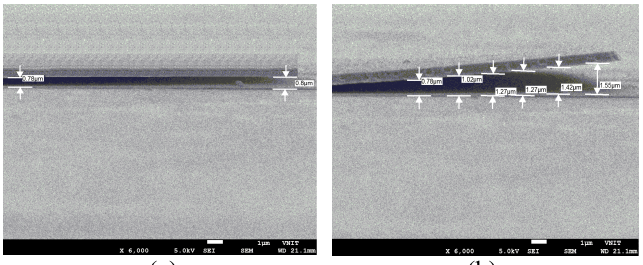

FIGURE 10. SEM image of (a) straight cantilever with gap of 0.8μm (b) curled cantilever with gap of 1.55μm.

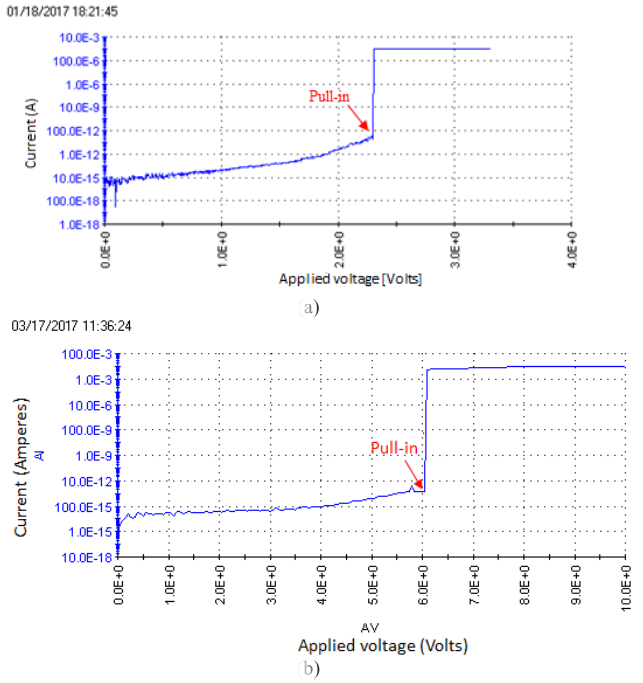

FIGURE 11. I-V characterization indicating the pull-in voltage of (a) 2.35 V for straight cantilever (b) 6.08V for curled cantilever.

The fabricated devices are characterized with help of Electrical characterization system consisting of Karl Suss shielded probe station, Source Measurement Unit (SMU) and Keithley 4200 Semiconductor characterization system [24] for current-voltage (I-V) measurements to obtain the pull-in voltage as shown in Fig. 11.

We took I-V measurements by applying ramp voltage from 0V to 10V between bottom electrode & top cantilever. For the set of straight cantilever beams, the current shoots up at voltage of 2.4V depicting switching phenomenon as shown in Fig. 11 (a). This is specified as pull-in voltage. At this, the beam snaps, causing cantilever and bottom electrode to come in contact and hence, a set compliance value of current passes through the device. For device safety, compliance value is provided to prevent its breakdown.

For the set of curled cantilever beam, pull-in voltage is obtained at 6.08V as shown in fig. 11(b).

Also, we observed that in Fig. 11, till the pull-in voltage is reached, there is a rise in current from fA to pA, which is due to the surface leakage current effect as discussed earlier. The leakage resistance modelled in circuit is calculated using the experimental results.

VI. CIRCUIT SIMULATION RESULT

The circuit simulation software NGSPICE is used for the simulation of the developed equivalent electrical circuit. The capacitance and transduction factors are modelled using the analog behavioural modelling function, which enables specification of polynomial functions.

DC analysis is performed on the circuit model for analysing response of MEMS cantilever beam to ramp-function voltage signal. The ramp-up time of signal needs to be chosen in such a way that circuit response time to each applied voltage is satisfied. The simulations are performed with ramp-up time 40ms (same timestamp as used in characterization) for voltage range of 0-5V. The simulation results obtained for DC analyses are as shown in Fig. 12 (a).

With voltage rise, electrostatic force and restoring force of cantilever comes into effect causing a rise in beam deflection, which results in the flow of current in the model. When restoring force dominates, cantilever shows stable deflection behaviour. This is portrayed by linear rise in current through transduction branch [$I(-C_1) = \Gamma I_m$]. At pull-in point, the effect of electrostatic force becomes dominant leading to loss of mechanical stability of cantilever and causes it to touch the bottom electrode. This is depicted as an abrupt increase

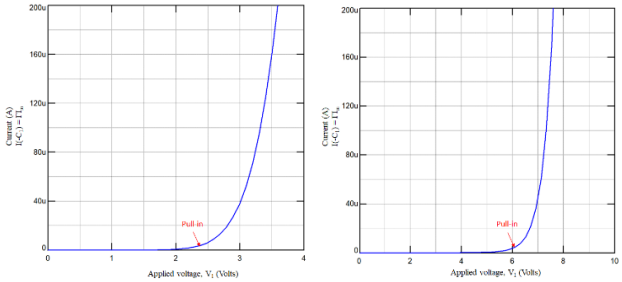

FIGURE 12. I-V curve obtained from circuit simulation for (a) straight cantilever (b) curled cantilever.

TABLE 3. Pull-in voltage comparison (wide beams).

E= 169GPa, w=50microns, t=3microns, g=1micron			
Beam length	100	100	150
Poisson's ratio	0.06	0.32	0.06
Vpi CoSolve FEA (experimentally verified) [25]	38.2	39.8	16.9
Vpi 2D Model [25]	37.9	39.9	16.8
Vpi Pull-in Model [19]	37.84	39.86	16.83 16.23
Vpi new theoretical model	36.5	38.5	6
Vpi new macro-model	36.8	38.9	16.5
% error between theoretical and CoSolve FEA [25]	4.45	3.26	3.9
% error between theoretical and 2D model [25]	3.69	3.5	3.35
% error between theoretical and pull-in model [19]	3.54	3.41	3.53
% error between macro-model and CoSolve FEA [25]	3.66	2.26	2.37
% error between macro-model and 2D model [25]	2.9	2.51	1.78
% error between macro-model and pull-in model [19]	2.74	2.4	1.96

TABLE 4. Pull-in voltage comparison (wide and narrow beams).

Common parameters : E= 77GPa, v= 0.33, g=2.5, t =1			
Width/Height ratio	> 5	>5	<5
length	300	500	300
width	50	50	0.5
Vpi [19]	2.27	0.8188	1.21
Vpi [25]	2.27	0.818	1.23
Vpi [26]	2.33	0.84	1.33
Vpi [CW FEA] [26]	2.25	0.75	1.2
Vpi CW Architect [19]	2.31	0.8125	1.2
Vpi[Theoretical]	2.19	0.7897	1.236
Vpi [Macro-model]	2.2	0.8	1.24
% error in theoretical & [19]	3.52	3.55	2.14
% error in theoretical & [25]	3.52	3.42	0.48
% error in theoretical & [26]	6	5.98	6.7
% error in theoretical & CW FEA [26]	-2.66	5.33	2.91
% error in theoretical & Architect [19]	5.19	2.81	2.91
% error in macro-model & [19]	3.08	2.3	2.48
% error in macro-model & [25]	3.08	2.2	0.8
% error in macro-model & [26]	5.58	4.76	6.7
% error in macro-model & CW FEA [26]	2.22	6.67	3.33
% error in macro-model & CW Architect [19]	4.76	1.54	3.33

in current flow. The onset of pull-in instability is marked by a change in the slope of the I-V curve. This corresponds to pull-in voltage of around 2.35 V.

Fig. 12 (b) gives the graph for I-V curve obtained when deformation due to curling is taken into consideration and put in (21) as per the measurements obtained from SEM images for fabricated device. It is observed that the pull-in voltage is around 6.05V, which matches with experimental and analytical results. Thus, methodology applied for lumped parameter estimation for development of the electrical equivalent circuit is capable to predict pull-in voltages for the curled beams also.

Comparing current flow of fig. 11 with fig. 12, we obtain higher current range in case of circuit model. This is due to the reason that in case of fabricated cantilever, large current flows, when pull-in occurs and cantilever touches the bottom electrode, which is a short. Both the graphs are comparative in a way that they provide information about the onset of pull-in phenomenon by predicting pull-in voltage.

VII. MODEL DISCUSSION AND VALIDATION

The results of macro-model simulation and the theoretical model developed in this paper has been additionally validated with the other previously published theoretical and experimental results. The experimentally verified CoSolve FEA results [25], wherein the authors used a Wentworth Labs probe station and an HP4145B Semiconductor Parametric Analyzer to measure the pull-in voltage of fabricated test structures with an accuracy of $\pm$ 100mV, was used as a benchmark for experimental comparison. The difference in the measured and CoSolve FEA result was reported to be 0.83%. Also, the 2D model presented in [25], closed-form analytical model presented in [19] are included for comparison in Table 3.

From Table 3, it is evident that the results obtained from the developed model are in good agreement with the experimentally measured values.

Table 4 shows the comparison of results of the present models with that of results published in [19], [25], and [26] for three more cases of different cantilever beam dimensions and material properties. It is observed that the pull-in voltages thus obtained are within 7% agreement with the previously compared models for both wide and narrow beams.

VIII. CONCLUSION

In this work, the macro model of electrostatically actuated MEMS cantilever beam is developed using the equivalent electrical circuit approach for design and analysis. Straight and curled cantilever beams are taken into consideration and lumped parameter estimation is done accordingly. The mechanical parameters are represented by electrical components. The transduction factor is analytically calculated considering coupled field effect. The model is then tested for system-level simulations and parameter evaluation. The results are verified with the analytical solution of governing equation and experimental results. The model accurately describes the pull-in phenomenon by predicting pull-in voltage. Thus, this macro model can be used for deploying MEMS cantilever in the circuits in the design flow of systems.

REFERENCES

[1] D. Rodrigo, Y. Damgaci, N. Biyikli, B. A. Cetiner, J. Romeu, and L. Jofre, "MEMS-reconfigurable antenna based on a multi-size pixelled geometry," in *Proc. 4th Eur. Conf. Antennas Propag. (EuCAP)*, Barcelona, Spain, Apr. 2010, pp. 1–4.

[2] C. Ong and M. Okoniewski, "MEMS-switchable microwave bandpass filter," in *Proc. 17th Int. Conf. Microw., Radar Wireless Commun.*, May 2008, pp. 1–4.

[3] B. A. Parviz, T.-K. A. Chou, C. Zhang, K. Najafi, M. O. Muller, P. D. Washabaugh, and L. P. Bernal, "Performance of ultrasonic electrostatic resonators for use in micro propulsion," in *Proc. 14th IEEE Int. Conf. Micro Electro Mech. Syst.*, Jan. 2001, pp. 586–589.

[4] G. Galambos, K. Zavadil, R. Givler, F. Peter, A. Gooray, G. Roller, and J. Crowley, "A surface micromachined electrostatic drop ejector," in *Proc. Transducers Eurosensors XV*, Munich, Germany, Jun. 2001, pp. 906–909.

[5] T. Mukherjee, K. Fedder, D. Ramaswamy, and J. White, "Emerging simulation approaches for micromachined devices," *IEEE Trans. Comput.-Aided Design Integr. Circuits Syst.*, vol. 19, no. 12, pp. 1572–1589, Dec. 2000.

[6] F. Wen, W. Li, Q. A. Huang, and H. Rong, "Large-signal lumped-parameter macro models for the equivalent circuit representation of electromechanical transducers," *J. Micromech. Microeng.*, vol. 14, no. 4, pp. 452–461, Jan. 2004.
[7] H. A. C. Tilmans, "Equivalent circuit representation of electromechanical transducers: I. Lumped-parameter systems," *J. Micromech. Microeng.*, vol. 6, no. 1, pp. 157–176, 1995.
[8] S. D. Senturia, "Simulation and design of microsystems: A 10-year perspective," *Sens. Actuators A, Phys.*, vol. 67, nos. 1–3, pp. 1–7, May 1998.
[9] S. D. Senturia, *Microsystem Design*. New York, NY, USA: Springer, 2001.
[10] H. A. C. Tilmans, "Equivalent circuit representation of electromechanical transducers: II. Distributed-parameter systems," *J. Micromech. Microeng.*, vol. 7, no. 4, pp. 285–309, 1997.
[11] W.-M. Zhang, H. Yan, Z.-K. Peng, and G. Meng, "Electrostatic pull-in instability in MEMS/NEMs: A review," *Sens. Actuators A, Phys.*, vol. 214, pp. 187–218, Aug. 2014.
[12] A. K. Sharma, R. K. Godara, and M. Joglekar, "Static and DC dynamic pull-in analysis of curled microcantilevers with a compliant support," *Microsyst. Technol.*, vol. 25, no. 3, pp. 965–975, Mar. 2018.
[13] M. Mita and H. Toshiyoshi, "An equivalent-circuit model for MEMS electrostatic actuator using open-source software Qucs," *IEICE Electron. Express*, vol. 6, no. 5, pp. 256–263, 2009.
[14] H. Toshiyoshi, "A spice-based multi-physics simulation technique for integrated MEMS," in *Proc. Int. Conf. Simulation Semiconductor Processes Devices (SISPAD)*, Osaka, Japan, Sep. 2011, pp. 239–242.
[15] H. Koymen, A. Atalar, E. Aydogdu, C. Kocabas, H. K. Oguz, S. Olcum, A. Ozgurluk, and A. Unlugedik, "An improved lumped element nonlinear circuit model for a circular CMUT cell," *IEEE Trans. Ultrason., Ferroelectr., Freq. Control*, vol. 59, no. 8, pp. 1791–1799, Aug. 2012.
[16] I. Ladabaum, X. Jin, H. T. Soh, A. Atalar, and B. T. Khuri-Yakub, "Surface micromachined capacitive ultrasonic transducers," *IEEE Trans. Ultrason., Ferroelectr., Freq. Control*, vol. 45, no. 3, pp. 679–690, May 1998.
[17] R. J. Roark and W. C. Young, *Formulas for Stress and Strain*. New York, NY, USA: McGraw-Hill, 1989.
[18] M. Akgul, L. Wu, Z. Ren, and C. T.-C. Nguyen, "A negative-capacitance equivalent circuit model for parallel-plate capacitive-gap-transduced micromechanical resonators," *IEEE Trans. Ultrason., Ferroelectr., Freq. Control*, vol. 61, no. 5, pp. 849–869, May 2014.
[19] S. Chowdhury, M. Ahmadi, and W. C. Miller, "A closed-form model for the pull-in voltage of electrostatically actuated cantilever beams," *J. Micromech. Microeng.*, vol. 15, no. 4, pp. 756–763, Feb. 2005.
[20] A. Ito, "A voltage dependent capacitance model including effects of manufacturing process variabilities on voltage coefficients," *IEEE Trans. Comput.-Aided Design Integr. Circuits Syst.*, vol. 14, no. 9, pp. 1093–1097, Sep. 1995.
[21] N. P. Van Der Meijs, and J. T. Fokkema, "VLSI circuit reconstruction from mask topology," *Integration*, vol. 2, pp. 85–119, Jun. 1984.
[22] R. Legtenberg, J. Gilbert, S. D. Senturia, and M. Elwenspoek, "Electrostatic curved electrode actuators," *J. Microelectromech. Syst.*, vol. 6, no. 3, pp. 257–265, Sep. 1997.
[23] J. Kalambe and R. Patrikar, "Design, fabrication, and characterization of electrostatically actuated microcantilever sensor for temperature detection," *IEEE Sensors J.*, vol. 15, no. 3, pp. 1595–1601, Mar. 2015.
[24] *4200 SCS Semiconductor Characterization System Technical Data by Keithley*, Keithley Instrum., Cleveland, OH, USA, Feb. 2009.
[25] P. M. Ostenberg and S. D. Senturia, "M-TEST: A test chip for MEMS material property measurement using electrostatically actuated test structures," *J. Microelectromech. Syst.*, vol. 6, no. 2, pp. 18–107, Jun. 1997.
[26] S. Pamidighantam, R. Puers, K. Baert, and H. A. C. Tilmans, "Pull-in voltage analysis of electrostatically actuated beam structures with fixed–fixed and fixed–free end conditions," *J. Micromech. Microeng.*, vol. 12, no. 4, p. 458, Jun. 2002.

AKANKSHA D. SINGH (S'16) received the B.Tech. and M.Tech. degrees from R.T.M. Nagpur University, Nagpur, in 2011 and 2013, respectively.

She served as an Assistant Professor for the Shri Ramdeobaba College of Engineering and Management, Nagpur, India in 2015. She is currently pursuing the Ph.D. degree with the Visvesvaraya National Institute of Technology, Nagpur. Her research interests include MEMS, digital design, device modeling, and fabrication of microdevices.

RAJENDRA M. PATRIKAR (SM'04) received the M.Tech. and Ph.D. degrees in electrical engineering from the Indian Institute of Technology (IIT) Bombay, Mumbai, India.

He joined the Faculty of IIT Bombay after working for one year at Computer Vision Research and Development, Pune, India. He was with the Department of Advance Device Technology, TECH Semiconductor Singapore Pte. Ltd. (currently Micron Semiconductor Asia Pte. Ltd.), Singapore, from 1998 to 2000, and the Institute of High Performance Computing, Singapore, from 2001 to 2003. He was a Team Leader with the Nanotechnology Group, Computational Research Laboratory, Pune, India, in 2008. He is currently a Professor of electronics with the Visvesvaraya National Institute of Technology, Nagpur, India. He has authored more than 40 articles in international journals and 90 articles in refereed conferences.

Prof. Patrikar is a Fellow of the IETE, a member of the International Society for Optics and Photonics, a Life Member of the Institute of Smart Structures and Systems, and a member of the International Society of Automation.